Thermochimica Acta 609 (2015) 49–60

Contents lists available at ScienceDirect

Thermochimica Acta

journal homepage: www.elsevier.com/locate/tca

Kinetics of depolymerization of paraformaldehyde obtained by thermogravimetric analysis

Edwing J. Grajales, Edwin A. Alarcón *, Aída L. Villa

Environmental Catalysis Research Group, Engineering Faculty, Chemical Engineering Department, Universidad de Antioquia UdeA, Calle 70 No. 52-21, Medellín, Colombia

ARTICLE INFO

Article history:
Received 22 January 2015
Received in revised form 15 April 2015
Accepted 17 April 2015
Available online 20 April 2015

Keywords:
Paraformaldehyde depolymerization
Thermogravimetrical analysis
Isoconversional method
Activation energy
Master Plot
Kinetic model

ABSTRACT

Solid paraformaldehyde is a source of formaldehyde that is preferred when anhydrous conditions in chemical processes are required. In this contribution, several depolymerization models were proposed for paraformaldehyde in powder (PFP) and prills (PFS), and they were validated with experimental thermogravimetric analysis (TGA). For description of PFP depolymerization, a model of a single step was adequate, and for PFS the best model included two simultaneous mechanisms. Kinetic models were determined using Master Plot method; for PFS, small intervals of conversion were used in order to obtain the best model at each finite point of the progress of reaction. Apparent activation energies (E_a) were obtained by isoconversional methods. For PFP, E_a was 31.7 kJ mol^{-1} and the model corresponded to Avrami-Erofeyev 2 (A2). For PFS decomposition, the activation energy of the two mechanisms was E_a = 105.4 kJ mol^{-1} for a contracting volume (R3) model and E_a = 48.4 kJ mol^{-1} for the Avrami-Erofeyev model.

1. Introduction

Formaldehyde, HCHO, is one of the simplest products of the methanol partial oxidation and one of the most reactive organic substances; hence, it is important in many reactions, for example as a raw material in polymerization processes [1]. In 2012 formaldehyde global production stood at 46.4 million tons [2]. HCHO is usually commercialized in aqueous solution, stabilized with methanol to avoid its polymerization, and in solid form as polymers: paraformaldehyde (PF) with 8–100 oxymethylene units or polyoxymethylene homopolymer (POM-H) with higher molecular weight, containing up to 500 or even more monomeric units [3]. PF is typically used as HCHO source when anhydrous reaction conditions are mandatory; for instance, for obtaining homoallylic alcohols from the Prins condensation of alkenes and HCHO [4]. This reaction has been widely studied to obtain nopol from β-pinene and PF over tin catalyst supported on mesoporous materials [5]. According to Table 1, nopol yield could be strongly affected by the specific properties of PF, in contrast to PF commercialized in powder, the nopol yield using PF commercialized in prills was lower and significantly affected by particle size. Furthermore, the activity of the catalytic system depends on the availability of *in situ* HCHO generation, which could be assessed by the kinetics of HCHO production from its polymers, information that is not deeply analyzed for PF in the open literature. An aim of this contribution is to understand the differences between PF commercialized in powder and in prills that could be related with nopol production.

Decomposition patterns are characteristic to each kind of polymer, and in some cases they can be used for identification purposes [8]. There are some reports about depolymerization analysis of POM-H [9–16], most of them using TGA but without detailed kinetic analysis; for PF the information is scarce [16,17]. As polyoxymethylenes (POM) is one the most important engineering polymers for automotive, mechanical, medical and consumer goods applications, its thermal decomposition has been readily studied; this process involves the stabilization by acetylating "—OH" chain ends, introducing comonomer in small proportions or using nanocomposite materials. The degradation of POM is carried out by stepwise thermal depolymerization from the chain ends, oxidative attack to produce hydroperoxides leading to chain scission and depolymerization, acidolytic cleavage in the presence of formic acid as a byproduct of HCHO oxidation, or thermal chain scission at elevated temperatures [18 and references therein].

Grassie and Roche [11], reported the former studies on depolymerization kinetics of POM-H by a technique known as thermal volatilization analysis (TVA), where pressure evolution is measured; the authors found that the degradation rate was proportional to the average molecular weight of the polymer raised

* Corresponding author. Tel.: +57 4 2196609; fax: +57 4 2191077.
E-mail address: edwin.alarcon@udea.edu.co (E.A. Alarcón).

http://dx.doi.org/10.1016/j.tca.2015.04.016
0040-6031/

to the 0.8 power. In an earlier work, Kern and Cherdron [16] found a pseudo-first order kinetics if PF (molecular weight of 1200 Da) was depolymerized by heating. More recently, Fray et al. [14] carried out TVA isothermal experiments to measure the pressure evolution until equilibria, obtaining that the initial rate of thermal depolymerization of POM-H was proportional to POM-H mass, and that the Arrhenius parameters depended on the POM-H sources, effect that was attributed to the differences of the chain length or impurities. In this contribution, detailed kinetics of depolymerization of PF, commercialized in powder and prills, was obtained by TGA, using a modification of the Master Plot method [19].

2. Experimental

2.1. Materials

Two sources of PF with 95% of purity, bought to Sigma–Aldrich, were used as received. PF in powder as fine particles, PFP (product number: 158127-500G, batch number: 11529JA), and PF in prills as spherical particles, PFS (product number: 441244-1KG, batch number: 7223CC).

2.2. Characterization of materials

PFP and PFS were characterized by X-ray diffraction (XRD), infrared spectroscopy, differential scanning calorimetry (DSC), and thermogravimetric analysis (TGA). XRD was carried out in a Bruker diffractometer D8 ADVANCE with CuKα radiation. For Fourier transform infrared spectroscopy (FTIR), pellets, prepared with controlled amounts of PF and KBr, were measured at room temperature in a SpectrumOne PerkinElmer instrument with a deuterated tri-glycine sulfate pyroelectric (DTGS) detector, at frequencies from 4000 to 400 cm^{-1} with a resolution of 4 cm^{-1}. DSC were obtained in a TA instrument model Q100 under nitrogen atmosphere; samples at room temperature were cooled to −80 °C at 20 °C min^{-1}, and the analyses were carried from −80 °C to 300 °C using a heating rate of 5 °C min^{-1}. The TGA experiments were carried out by non-isothermal method using a Q-500 TA instruments; the samples, with mass between 10 and 15 mg, were heated at three different heating rates $\beta = 5$, 7.5 and 10 °C min^{-1}, with a continuous nitrogen flow of 40 mL min^{-1} from 20 to 300 °C.

3. Results and discussion

3.1. Characterization of paraformaldehyde

3.1.1. Structure and morphology

As POM-H with low polymerization degree is called PF, POM-H will be taken as a reference for the analysis of PF. Actually, PF exhibits almost the same XRD pattern and infrared spectrum as POM-H, which suggests that the molecular and crystal structures

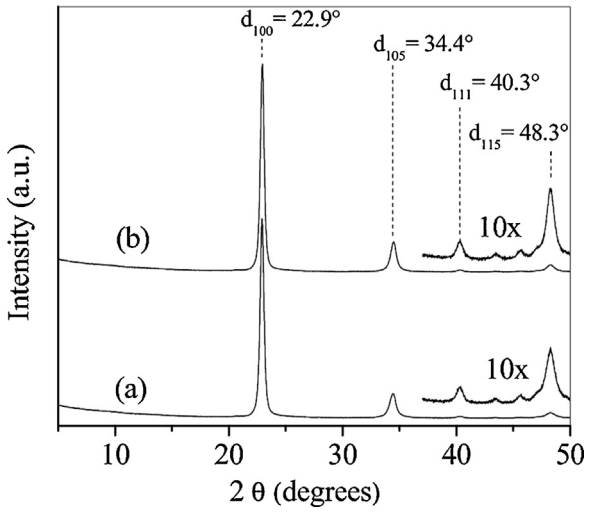

Fig. 1. XRD of paraformaldehyde samples. (a) PFP and (b) PFS.

of these two materials are very similar [20,21]. Fig. 1 shows the main peaks and diffraction to planes [22] in agreement to those reported for POM [23], and are close to the calculated positions for POM-H in the 2θ scan about $d_{100} = 22.9°$, $d_{105} = 34.6°$ and $d_{115} = 48.4°$ [18]; then, both PFP and PFS samples consist of hexagonal crystals with chains in helical conformations, which are the structural characteristics reported for POM [18]. The apparent crystallite size (ACS) [23] of the PF samples analyzed in this contribution and calculated according to the Scherrer equation, Eq. (1), is shown in Table 2. As the crystallite size of PFS was about 2% higher than PFP, it is possible to suggest that significant differences are not obtained at crystal level for both PFP and PFS samples; however, crystal sizes of PF samples analyzed in this contribution were higher that reported POM crystal size (Table 2, line 3).

$$\mathrm{ACS} = \frac{K\lambda}{(\Delta 2\theta)\cos\,(\theta)} \tag{1}$$

where K is a constant related to crystallite size taken as 1, λ is the wavelength (0.15418 nm), $\Delta 2\theta$ is the integral breadth (ratio between peak area and peak height in radians), and θ is the corresponding peak angle.

Fig. 2 shows that the majority of the bands in the FTIR spectra for both PFP and PFS samples are common; furthermore, those bands have been reported in the literature for POM [20,21,23–25]. Although there are some bands that have not been identified yet, important differences between the two PF samples are observed. It has been reported that the intensity of the 903 cm^{-1} band is proportional to the degree of polymerization [20]; however, no significant difference was found for this band in the samples analyzed. The morphological structure of crystalline POM-H, at a scale lower than micrometer level but higher than crystal lattice, may be classified as extended-chain crystals (ECCs) and folded-

Table 1
Activity on nopol synthesis with different sources of solid PF over catalytic system based on Sn-MCM-41. Adapted from Ref. [6].[a]

Time, (min)	dp, (μm)[b]	Yield PF in powder, (%)[c]	Yield PF in prills, (%)[c]
2	58	12.5	5.0
2	338	11.5	1.8
5	58	23.0	10.2
5	338	19.9	2.7

[a] Reaction conditions: 0.25 mmol β-pinene, 0.5 mmol PF, 2.2 mg sieved catalyst (Sn-MCM-41 obtained by hydrothermal method with tin loading of 43 μmol g^{-1} [7]), 0.5 mL toluene, 90 °C, stirring rate 1000 rpm.
[b] Average between sizes of standard series mesh.
[c] Further description of these samples in Section 2.1. The standard deviation of measurements was in average 1.1% units.

Table 2
XRD parameters of peak corresponding to plane d_{100}.

Sample	d_{100} position 2θ, (°)	FWHM, (°)[b]	ACS, (nm)[c]
PFP	22.92	0.394	17.57 (20.60)
PFS	22.96	0.390	17.98 (20.78)
POM[a]	23.00	0.699	13.0 (12.9)

[a] Copolymer F30-03 as reported in Ref. [23].
[b] FWHM: full width at half maximum.
[c] In parenthesis the crystallite size obtained with Eq. (1) using FWHM instead of integral breadth and $K = 0.9$.

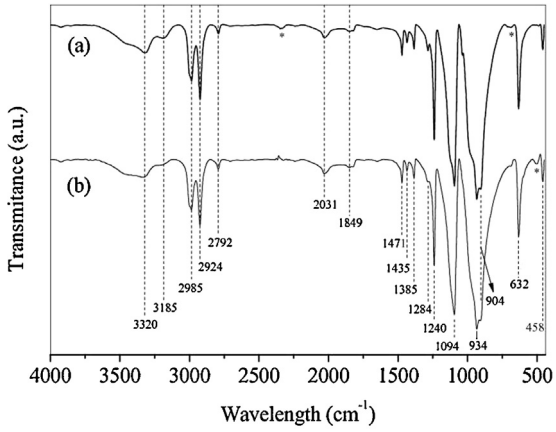

Fig. 2. FTIR analysis of PF samples (a) PFP and (b) PFS. *Unidentified bands.

chain crystals (FCCs); those structures show essentially the same XRD pattern, but they may be clearly distinguished by FTIR spectroscopy because of the high sensitivity of this technique to morphological changes [18,26–28].

As many bands of PFP and PFS overlapped each other, the spectra was differentiated twice with respect to wavenumber for separating the sharp bands of the crystalline phase from the broad bands of the amorphous region [26],Fig. 3. The peaks at 633, 935 and 1239 cm^{-1} are assigned to both ECC and FCC crystal morphologies. Bands at 900 and 1090 cm^{-1} belong only to the ECC morphology; they show the same intensity in both samples. As bands at 998 and 1138 cm^{-1} that are assigned only to the FCC morphology are more intense for PFP, then this type of PF counts with a major contribution of the FCC structure respect to PFS.

3.1.2. Thermal analyses

Figs. 4 and 5 show TGA and DTG curves, respectively, at different heating rates for PFP and PFS samples. TGA curves show different consumption rates through time depending on the heating rate. Although the shape of the curves corresponds to thermal decomposition toward volatile compounds, they also have the shape of drying processes or desorption of other substances such as solvents or monomers [29]. Considering the nature of the samples, it is expected that during the TGA, the decomposition to volatile compounds such as HCHO occurs; in fact, in the absence of oxygen, it has been confirmed by IR spectroscopy that HCHO is the single product of POM-H depolymerization [14]. Furthermore, HCHO has been detected as the main product from TGA under nitrogen atmosphere of POM copolymers with hydroxyl chain-ending [30–32]. TGA of PF samples did not show events related with impurities.

It has been reported that gaseous HCHO is slowly polymerized below 100 °C [3]; hence, it is reasonable to conclude that both PFS and PFP samples were completely decomposed at the maximum temperature tested. Although residual solid is commonly observed in TGA due to incomplete reactions [33], Fig. 4 shows that residual mass was not left upon decomposition for all the heating rates and PF samples, in agreement with TGA of POM-H [13,15]. However, the decomposition onset temperatures of PFP were lower than values for PFS, Table 3, with an average difference of about 36 °C, and for both PF samples the values were significantly lower than those reported with solids such as POM-H at $\beta = 10\,^{\circ}C\,min^{-1}$. Similar conclusions come from comparison of DTG curves of PFS, PFP and POM-H samples (Fig. 5, Table 3). The maximum weight loss temperatures obtained from DTG curves were directly related to the heating rate in both PF samples, with an average difference in favor of PFS of around 26 °C. At $\beta = 10\,^{\circ}C\,min^{-1}$ the corresponding

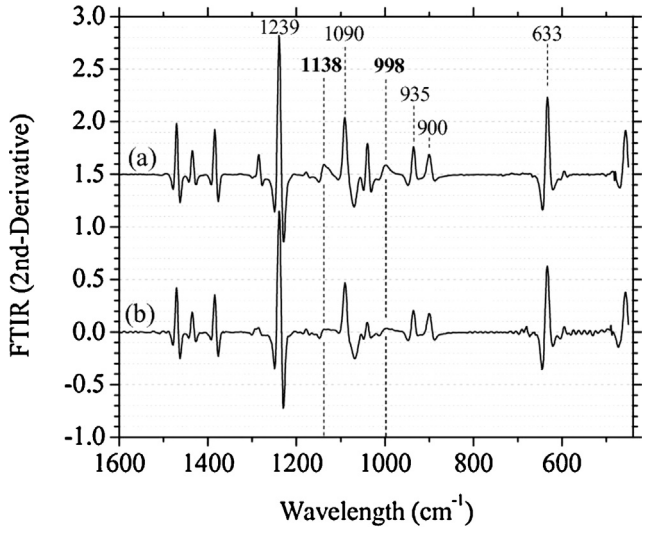

Fig. 3. Second derivative of FTIR curves for (a) PFP and (b) PFS. Curve (a) with 1.5 units vertical offset.

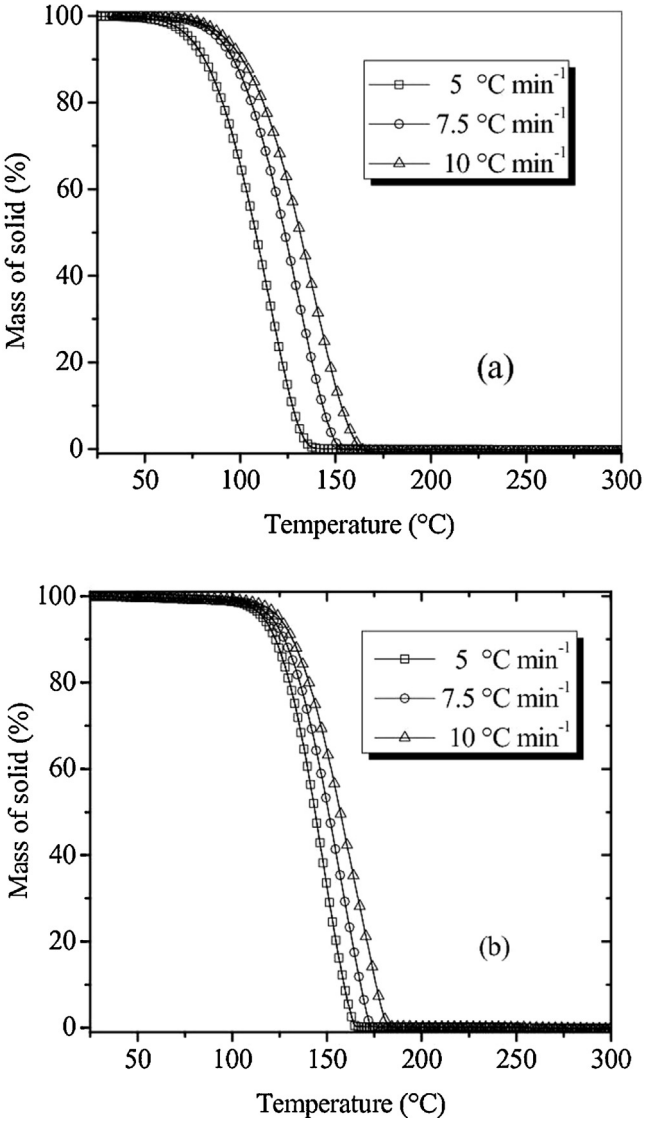

Fig. 4. Effect of the heating rate on the decomposition of paraformaldehyde. (a) PFP, and (b) PFS.

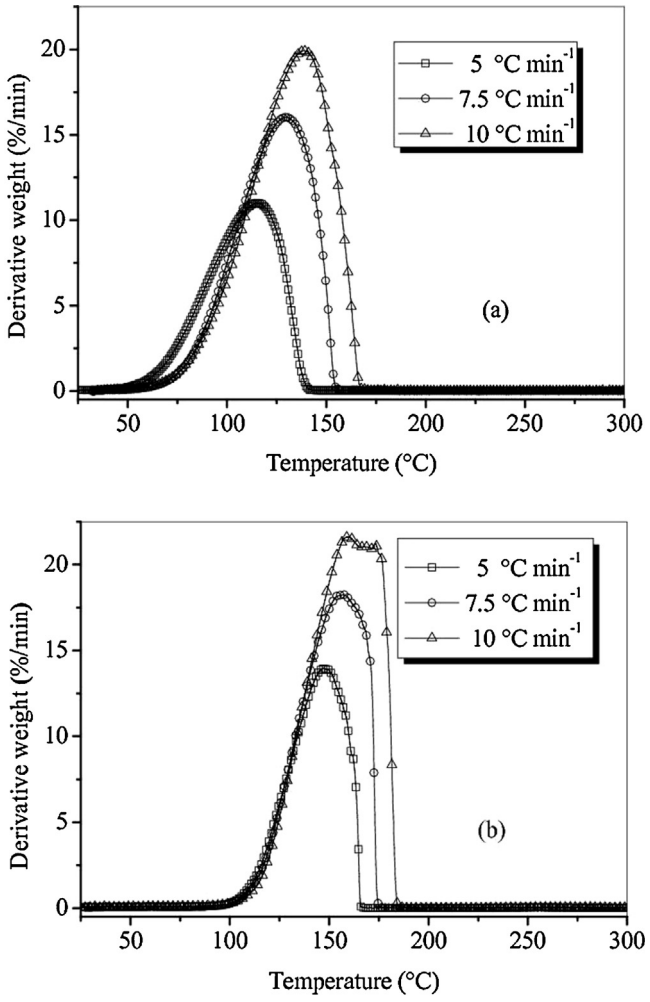

Fig. 5. DTG curves of the decomposition of PF. (a) PFP, and (b) PFS.

values for samples of POM-H were at least twice the value of PFS. Longer homopolymer chains of POM-H [11,16,18] have been inversely related to the degradation rate, with shift to higher values of T_{onset} and T_m temperatures, which explain the strong differences between PF and POM-H in Table 3. These imply that chain-end scission mechanism governs the depolymerization in our samples in nitrogen atmosphere instead of random chain scission and acidolytic cleavage, which are favored in the presence of oxygen and shows a proportional relationship between molecular weight of POM and degradation rate [13,18,32]. These findings suggest that the slower depolymerization rate of PFS respect to PFP could be associated to a higher molecular weight of PFS. Moreover, the higher contribution of FCC morphology of PFP could be also in agreement to higher degradation rate, since the FCC structure may be considered as imperfect crystals, with about 20% amorphous part concentrated at the fold surface [34], with stems shorter than ECC and with folded-chain segments on two opposite sides, which melts a POM-H sample at a temperature lower than ECCs [18].

DSC analysis of PF samples (Fig. 6) did not show any signal related to a glass transition or a melting point, typical of POM-H [18], but the corresponding signals were coherently related to a degradation pattern, similarly to that observed in the work of Kusy and Whitley [15]. The calculated gasification enthalpies (h_g) were 1.994 and 2.066 kJ g^{-1} for PFP and PFS, respectively, which are not significantly different (only 3.6% higher respect to PFP), and are in the same order of magnitude of average h_g for pyrolysis of several polymers (2.0 ± 0.5 kJ g^{-1}), but quite different to the compiled value of POM (2.4 kJ g^{-1}) [35]. On the other hand, DSC pattern of PFP exhibited a signal at around 40 °C which is not associated to its degradation process, but which might be related to the formation of the ECC structure or the straight tie chains passing through the neighboring lamellae [36], whose intensity becomes higher on a FTIR spectra after decreasing temperature [26]. This finding suggests that higher depolymerization rate of PFP respect to that of PFS, under nitrogen atmosphere, is more probably related to the differences on molecular weights than on the presence of amorphous phases, which has been related with the enhance of the thermo-oxidative decomposition rate of acetylated POM [34,37] or POM-copolymers [38].

Fig. 4 suggests that decomposition process occurred in single or parallel reactions, instead of successive reactions, as in TGA several inflection points are not observed [39]. The presence of a pronounced shoulder in the DTG, Fig. 5(b) for $\beta = 10$ °C min^{-1}, and DSC, Fig. 6, could suggest the presence of parallel reactions for PFS as it will be shown in the next sections.

Table 3
Thermal parameters from TGA and DTG of PF and POM-H samples.

Sample	β, (°C min^{-1})	T_{onset}, (°C)[a]	T_m, (°C)[b]
PFP	5	68.09	114.81
	7.5	83.36	129.92
	10	85.84	138.50
PFS	5	111.51	146.79
	7.5	115.42	156.68
	10	119.81	159.16
POM-H[c]	10	326	390
POM-H[d]	10	255	325

[a] Onset temperature corresponding to 3% weight loss as recommended in Ref. [13].
[b] Temperature of the maximum position in DTG.
[c] Data taken from Ref. [13] for a POM-H supplied by DuPont.
[d] Estimation from Ref. [15] for a POM-H Delrin.

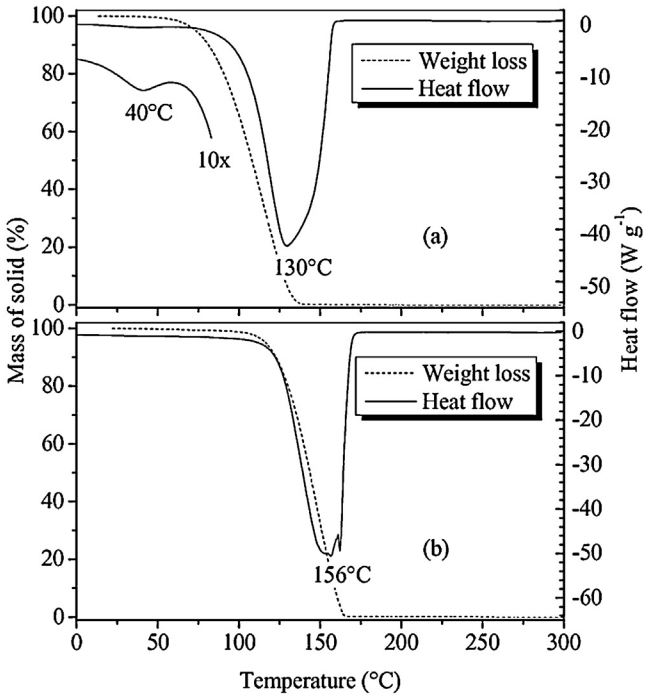

Fig. 6. TGA and DSC analyses of PF samples with heating rate of 5 °C min^{-1}. (a) PFP, inset: DSC signal multiplied by 10, and (b) PFS.

3.2. Kinetic analyses

3.2.1. Determination of the activation energy for PFP

The general kinetic law for decomposition reactions in solids is usually described by Eq. (2). This expression is used for single reaction processes, as it is the case of PFP depolymerization.

$$\frac{d\alpha}{dt} = k(T) \times f(\alpha) \tag{2}$$

where $f(\alpha)$ is a function that depends on the reaction mechanism; α is the conversion, Eq. (3), and $k(T)$ is the rate constant, Eq. (4).

$$\alpha = \frac{m_0 - m_t}{m_0 - m_f} \tag{3}$$

$$k(T) = A \times \exp\left(\frac{-E}{RT}\right) \tag{4}$$

Here, m_0 is the initial mass, m_t is the mass in the time t, m_f corresponds to the residual mass. Regarding to the rate constant, A is the pre-exponential factor, E represents the activation energy, R is the universal gas constant and T is the absolute temperature [38].

The isoconversional methods are the most used to compute activation energy because they can be applied to polymers with complex degradation mechanisms [38]. The isoconversional principle states that the reaction rate at constant conversion is only a function of temperature [39], or, in others words, establishes that the reaction model $f(\alpha)$, is independent on the heating rate [40]. Isoconversional methods are frequently called "model-free" methods because they allow to evaluate the activation energy for a specific conversion degree, $E\alpha$, without assuming any particular form of $f(\alpha)$. Nevertheless, it is important to assume that the conversion dependence of the rate obeys some $f(\alpha)$ model [39].

Integral and differential isoconversional approaches are usually used to calculate the activation energy. For constant heating rate, from Eqs. (2) and (4) we can obtain Eq. (5), which is the basis of integral isoconversional method.

$$g(\alpha) \equiv \int_0^{\alpha} \frac{d\alpha}{f(\alpha)} = \frac{A}{\beta}\int_0^{T} \left(\frac{-E}{RT}\right) \times dT = \frac{A}{\beta}\tau(T) \tag{5}$$

Eq. (5) does not have analytical solution and different approximations have been proposed [39]. A popular solution considers that $2RT/E$ is much lower than unity and it is called Kissinger–Akahira–Sunose (KAS), Eq. (6).

$$\ln\left(\frac{\beta}{T^2}\right) = \ln\left(\frac{A \times R}{g(\alpha) \times E_\alpha}\right) - \frac{E_\alpha}{RT} \tag{6}$$

For each degree of conversion at different heating rates (β), the linear plot of $\ln(\beta/T^2)$ *vs.* $1/T$ facilitates the calculation of E_α and $\ln[A \times R/(g(\alpha) \times E_\alpha)]$ from the slope and the intercept, respectively [38].

On the other hand, the Friedman method (FR) is the most common differential isoconversional method, and is based on Eq. (7) which is obtained from Eqs. (2) and (4).

$$\ln\left(\frac{d\alpha}{dt}\right)_{\alpha,i} = \ln[f(\alpha) \times A_\alpha] - \frac{E_\alpha}{R \times T_{\alpha,i}} \tag{7}$$

For a constant α, the plot of $\ln(d\alpha/dt)$ *vs.* $1/T$ obtained from curves recorded at several β, labeled with i, should be a straight line whose slope correspond to the value of E_α [38].

The dependency of activation energy for conversion degrees between 0.05 and 0.95, using KAS and FR methods, is shown in Fig. 7. The determination coefficients, R^2, for evaluation of E_α for each α, are below 0.98 for $\alpha < 0.6$ using the integral method with a minimum of $R^2 = 0.90$ for $\alpha = 0.05$. In contrast, R^2 are above 0.99 when a differential approach was used, indicating a good quality of the experimental TGA data. Values of E_α from integral method showed deviations below 3% respect to the mean. These findings suggest that complex integration for treatment of data are not necessary in the evaluation of E_α [39]. Although FR method had better correlation for each conversion degree, values of E_α are oscillating at around 10% deviation respect to the average of higher and minimum values. This deviation could be attributed to either the difficult determination of baseline or the noise increment after differentiation of experimental data, associated to differential methods. These variations levels have been observed in the treatment of TGA data for calcium carbonate, which showed E_α between 180 and 220 kJ mol^{-1}[41]. Moreover, it is important to note that the nearly constant profile of E_α with conversion in nitrogen is in agreement to the results reported by Lüft et al. [42] using an POM copolymer, whose values, obtained by the method reported by Flynn and Wall [43], were nearly constant at 150 kJ mol^{-1} or higher values depending on the treatment of the polymer, which is coherent to the effect of adjacent carbon–carbon of copolymer; for comparison purposes the method of Flynn and Wall with our data produced a similar trend of E_α with conversion, but E_α respect to KAS method for PFP and PFS were overestimated in average 15 and 4%, respectively. The authors reported that for higher conversion degrees, activation energies lowered continuously under air atmosphere while they remained nearly constant under nitrogen atmosphere; that difference was mainly associated to the degradation mechanism. Under oxygen, the scission and autocatalytic type mechanism are probably occurring simultaneously, and in nitrogen mainly thermal induced depolymerization after the chain scission occurs, as it was previously discussed in Section 3.1.2.

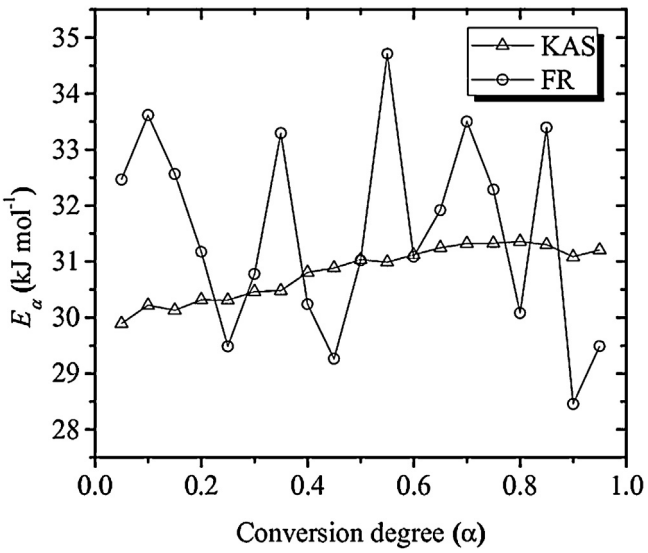

Fig. 7. Effect of the conversion degree on activation energy evaluated by KAS and FR isoconversional methods for PFP.

Table 4
Statistical parameters for activation energy obtained from KAS and FR methods for PFP.

Parameter	KAS	FR
Average activation energy, E_{mean} (kJ mol^{-1})	30.8	31.5
Standard deviation, SD (kJ mol^{-1})	0.5	1.8
Coefficient of variation, CV (%)	1.5	5.6

The average activation energy for KAS and FR methods are too close each other with a difference of around 0.7 kJ mol^{-1} (Table 4). If activation energies were not similar for both methods, a significant variation of E_α with conversion would be expected [38]. Then, our results support the idea of having constant activation energy with conversion, indicating that either single or simultaneous reactions are occurring, as indicated previously from thermogravimetric analysis (Section 3.1). Regarding to this aspect, Vyazovkin et al. showed that if E_α is relatively constant in the whole conversion range, then the process is dominated only by one reaction step [39].

Since parallel reactions could probably be occurring, it was checked through the calculation of activation energy by the lineal methods of Kissinger [39] and Farjas [41]. The Kissinger equation, Eq. (8), can be obtained from Eqs. (2) and (4) under the maximum reaction rate condition, where second derivative, $d^2{}_\alpha/dt^2$, is zero. In this method, left side of Eq. (8) is plotted *vs.* $1/T_m$ giving a straight line, where m indicates the maximum position or maximum velocity (Fig. 5a). A limitation of this method is that the accurate determination of activation energy requires $f'(\alpha_m)$ to be independent of β, otherwise deviation from linear fitting could be observed and a systematic error in the calculation of E_α is obtained. Another limitation of the method is that the activation energy is computed without taking into account the complexity of the kinetic process [39].

$$\ln\left(\frac{\beta}{T_m^2}\right) = \ln\left(-\frac{A\times R}{E}\times f'(\alpha_m)\right) - \frac{E}{R\times T_m} \quad (8)$$

To evaluate the occurrence of simultaneous reactions, Farjas et al. [41] showed that the peak width in DTG analysis is sensible to the deviations respect to kinetic model reactions. The authors found an analogous equation to Kissinger (Eq. (9)); then, a combined plot of Kissinger and Farjas should provide a reliable determination of the activation energy [39]. In fact, if only one reaction occurs, the obtained activation energies with each method should be almost the same [41].

$$\ln(\Delta t_{FWHM}) = \frac{E}{R\times T_P} + \ln\frac{\Delta t'_{FWHM}}{A} \quad (9)$$

where Δt_{FWHM} is the full width at half maximum in time units and $\Delta t'_{FWHM}$ is its normalized value.

Table 5 and Fig. 8 show a good agreement of the Kissinger and Farjas methods with experimental data. The variation in conversion was not significant, Table 5, and therefore the assumption of the Kissinger method that $f'(\alpha_m)$ is constant, could be adequate. Strictly, the conversion is independent among different heating rates for the first order kinetic model, $f'(\alpha_m) = -1$; furthermore, variation in α with β is not appreciable for power law and Avrami-Erofeyev models (Table 6) [39]. Therefore, the depolymerization of PFP could obey some of these three kinds of models.

Activation energies obtained from Kissinger and Farjas methods were 31.7 ± 2.8 and 32.5 ± 1.8 kJ mol^{-1}, respectively, with a difference between those values of around 2.5%; therefore, there the depolymerization is carried out in only one step [41].

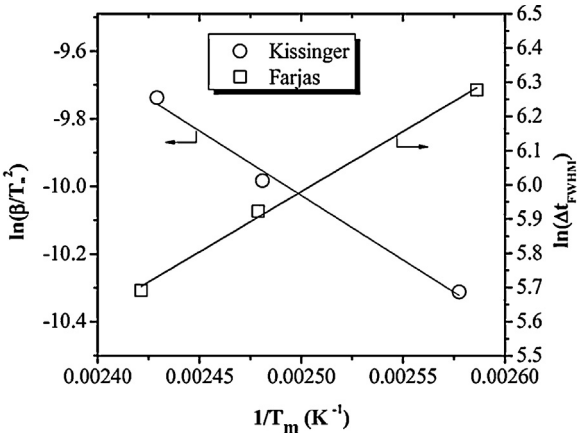

Fig. 8. Plots of the Kissinger and Farjas methods to estimate the activation energy for PFP. Continuous lines correspond to linear fitting and symbols to experimental data.

Furthermore, the values are relatively close to E_{mean} obtained for the KAS (30.8 kJ mol^{-1}) and FR (31.5 kJ mol^{-1}) isoconversional methods (Table 4). In fact, according to the standard deviation of the four values are the same from statistical point of view. Because of this, the estimated and averaged activation energies correspond to an apparent parameter in the whole conversion range.

3.2.2. Determination of the activation energy for PFS

KAS and FR methods were also followed for the analysis of experimental data of PFS. In contrast to PFP, in the whole range of α, the KAS method was better than the FR method with a R^2 above 0.99. With the differential method, the R^2 values varies between 0.89 (for $\alpha = 0.95$) and 0.98 for $\alpha > 0.65$. Fig. 9 shows that the activation energy changed in a broad range for both KAS and FR methods; for instance, it changed from 60 to 100 kJ mol^{-1} for KAS method. The deviations of maximum and minimum values of $E\alpha$ respect to the mean value, were 36 and 56%, for KAS and FR, respectively. The International Confederation for Thermal Analysis and Calorimetry (ICTAC) [39] suggests the use of more complex integral or differential methods when these variations are above 20–30%. Integral methods solve $\tau(T)$ in Eq. (5) with the assumption of E_α constant between integration limits, but in the practice E_α could change with conversion [39,45], as observed in these results.

On the other hand, the apparent activation energy, E_a, was determined by the Kissinger and Farjas methods (calculations not shown). As E_a obtained from Kissinger (68.5 kJ mol^{-1}) and Farjas (51.1 kJ mol^{-1}) methods were quite different, then it is concluded that a kinetic analysis involving more than one step should be applied for PFS.

When multiple steps are involved in the process, the global conversion can be described by Eq. (10) [39].

$$\frac{d\alpha}{dt} = k_1(T)\times f_1(\alpha_1) + k_2(T)\times f_2(\alpha_2) \quad (10)$$

Table 5
Experimental data for evaluation of the Kissinger and Farjas method for PFP.

Entry data				Linear fitting		
β, (°C min^{-1})	T_m, (K)	α_m	Δt_{FWHM}, (s)	Parameters	Kissinger	Farjas
5	387.96	0.6452	532.5	Slope	−3813.2	3911.4
7.5	403.07	0.6384	373.5	Intercept	−0.4937	−3.7984
10	411.65	0.6397	296.5	R^2	0.9921	0.9974

Table 6
Differential, $f(\alpha)$, and integral, $g(\alpha)$, expressions for different reaction models [44].

Mechanism	Model	$f(\alpha) = 1/k\ d\alpha/dt$	$g(\alpha) = kt$
Nucleation	Power law (P2)	$2\alpha^{1/2}$	$\alpha^{1/2}$
	Avrami-Erofeyev (A2)	$2(1-\alpha)[-\ln(1-\alpha)]^{1/2}$	$[-\ln(1-\alpha)]^{1/2}$
	Prout–Tompkins (B1)	$\alpha(1-\alpha)$	$\ln[\alpha/(1-\alpha)] + c^{\alpha}$
Geometrical contraction	Contracting area (R2)	$2(1-\alpha)^{1/2}$	$1-(1-\alpha)^{1/2}$
	Contracting volume (R3)	$3(1-\alpha)^{2/3}$	$1-(1-\alpha)^{1/3}$
Diffusion	1-D diffusion (D1)	$1/(2\alpha)$	α^2
Pseudo-order	First-order (F1)	$(1-\alpha)$	$-\ln(1-\alpha)$

where α_1 and α_2 are the specific conversion degrees associated to the two individual parallel reactions and α is the overall conversion.

Vyazovkin published the use of integral methods to evaluate the activation energy, when complex reactions occur [40,46,47]. These methods are useful if lineal methods fail in the calculation of E_α, and there is not evidence of multiple reactions. The author developed a method that accounts the variation of the activation energy with the conversion [20]. The activation energy is calculated minimizing the objective function given by Eq. (11) [47]:

$$\Phi(E_\alpha) = \sum_{i=1}^{n}\sum_{j\neq i}^{n}\frac{J[E_\alpha, T_i(t_\alpha)]}{J[E_\alpha, T_j(t_\alpha)]} \tag{11}$$

where the integral of temperature is:

$$J[E_\alpha, T_i(t_\alpha)] \equiv \int_{t_\alpha-\Delta\alpha}^{t_\alpha} \exp\left[\frac{-E_\alpha}{R \times T_i(t)}\right] dt \tag{12}$$

Eq. (12) can be solved numerically; a minimization is carried out for each value of α to obtain a dependence of E_α. Narrow integration intervals, $\Delta\alpha$, allow to obtain the average activation energy into small intervals, different to others numerical integrations such as KAS method, where normally the kinetic parameter average is computed in broad intervals $(0-\alpha)$, and E_α undergoes an undesirable flattening [47]. Therefore, Eqs. (11) and (12) were used in this work to compute E_α for PFS, which is called the modified non-linear (MNL) method.

Fig. 10 shows the dependency of activation energy with conversion using MNL [47] and FR methods for $\alpha = 0.02$–0.98 with steps of 0.01. It is clear that both methods resulted in similar values, in agreement with observations of other authors [48,49]. As aforementioned, the pattern in Fig. 10 is typical of a complex decomposition mechanism with multiple reactions [39,40,48,50]; however, by TGA is possible to propose a "kinetic scheme" [50], but no a mechanism approach which requires to use TG-MS [51].

The shape of the curve in Fig. 10 allows inferring the kinetic scheme. For example, growing curves have been associated to thermal decomposition of lineal polymers which decompose through weak bonds, such as peroxide and hydroperoxide, followed by decomposition through free radicals [45]. From the relationship between E_α and α, some models have been identified [50]: competitive [52], independent [53], consecutive [54], reversible reaction [55], and diffusional controlled models [56]. The competitive reactions have an increasing trend, which is a natural consequence of the exponential relationship of temperature and the specific reaction rate [53]. Vyazovkin studied in detail some examples of parallel reactions occurring independently [53]; in those cases, a dependency of E_α and α in increasing pattern like a "*S*" or sigmoidal was obtained, or a decreasing relationship with an inflection point, or a concave dependency. Neither growing, competitive nor independently reactions are related to the depolymerization of PFS.

The descending concave curve is partially adapted to a thermal reversible decomposition followed by an irreversible reaction, the latter being the controlling step [55]. If the process were reversible, E_α and α relationship would show an approximately decreasing lineal dependence, with $E\alpha$ between the corresponding values of direct and inverse reaction [55]. Diffusional controlled kinetics show a decreasing convex trend of E_α and α, because the increment of temperature accelerates the formation of gaseous intermediate going to a diffusive regime, in which low activation energies are observed. At the beginning, the decomposition is governed by the

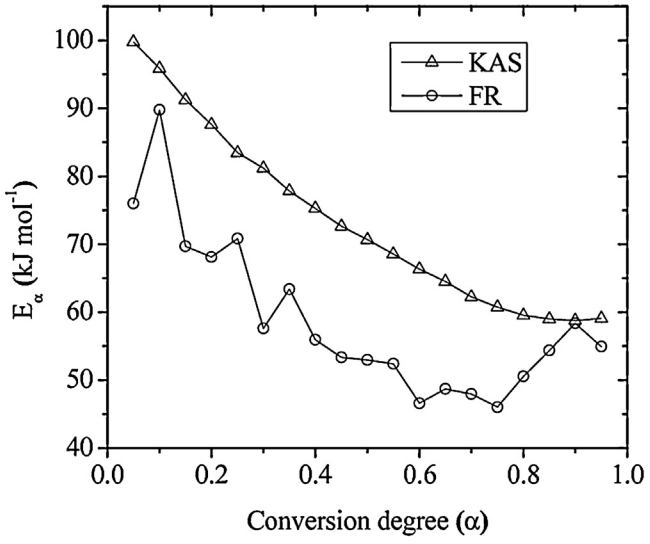

Fig. 9. Effect of the conversion degree on activation energy evaluated by KAS and FR isoconversional methods for PFS.

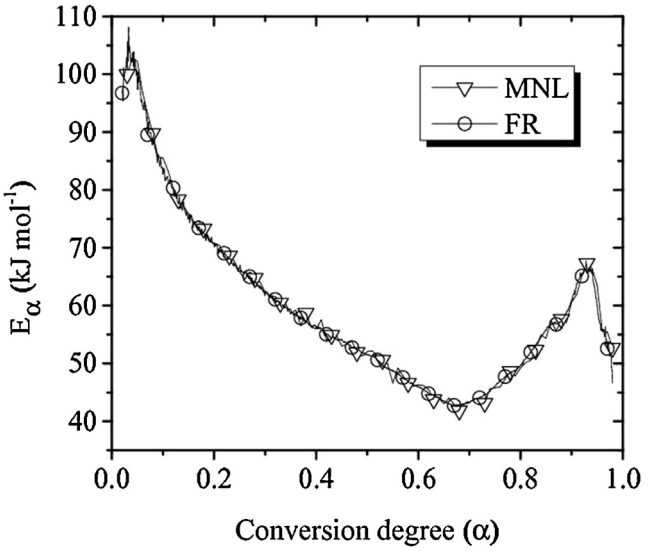

Fig. 10. Effect of the conversion degree on activation energy evaluated by MNL and FR methods for PFS.

chemical reaction, and not by diffusion; for this reason, E_α and α should be practically constant starting the analysis [56]. Then, profiles of Fig. 10 are closely associated to either reversible or diffusional models. Finally, consecutive reactions shows multiple experimental profiles [54].

The aforementioned cases do not explain the peak form observed after $\alpha > 0.65$ (Fig. 10). It is known that HCHO and its polymer could be in equilibrium (Reaction (R1)) [57–59], but under TGA conditions the nitrogen flow and the heating rate, which allow high temperature in almost all the process, domains against the reversible step. It is recognized in the real analysis, the curves could be indistinguishable to obtain the kinetic scheme [53]; moreover, the prior studies on kinetic schemes were based on first order kinetics, and the weighting of contributions of reaction and thermal effects are the same. Therefore, it is clear that TGA could be enough complex and particular interpretations arising from one case to other. In the next sections, a kinetic scheme for depolymerization of PFS is proposed.

$$R\text{–}OH + CH_2O \leftrightarrow ROCH_2OH \quad (R1)$$

3.2.3. Kinetic model determination for PFP

In the literature, different graphical methods have been reported to obtain reaction models of solids from TGA: the differential method or $Y(\alpha)$ function, the integral method, and the combined method or $Z(\alpha)$ function, which are called the Master Plot [19,60]. In many cases, experimental kinetic data can be transformed easily to Master Plot experimental curves. Comparison of these curves with theoretical Master Plots allows to choose the appropriate mechanism or, at least, the convenient kinetic [19]. The solid decomposition kinetic models are comprised by nucleation, geometrical contraction, diffusion and reaction-order models, which are summarized in the work of Khawam and Flanagan [44]. To use the Master Plot method the process must have only one reaction, then, the kinetic parameters should keep relatively constant on whole conversion range [39], as it is the case of PFP depolymerization (see Section 3.2.1).

When data are in integrated form, like TGA data, it is recommended to use the integral form of the generalized kinetic equation, Eq. (13).

$$\frac{g(\alpha)}{g(0.5)} = \frac{\theta}{\theta_{0.5}} \quad (13)$$

For a constant heating rate, the value of θ to a given conversion α can be obtained with Eq. (14). $\theta_{0.5}$ is the value of Eq. (14) to a conversion of 0.5.

$$\theta = \frac{E}{\beta \times R} \times p(x) \quad (14)$$

where $x = E/(RT)$, and $p(x)$ represents the temperature integral that although cannot be exactly solved, a convergent series can be used to approximately calculate it (Eq. (15)) [61].

$$p(x) = \frac{e^{-x}}{x}\pi(x) \quad (15)$$

where $\pi(x)$ is given by Eq. (16).

$$\pi(x) = \frac{x^3 + 18x^2 + 86x + 96}{x^4 + 20x^3 + 120x^2 + 240x + 120} \quad (16)$$

If the activation energy is defined (31.7 kJ mol^{-1} from Kissinger method) the decomposition models will not require several TGA. However, the treatment of our experimental data at the three heating rates resulted in similar conclusions. For instance, Fig. 11 illustrates the curves obtained for $\beta = 10\,^{\circ}C\,min^{-1}$, including the most representative and well fitted models (Table 6). This figure

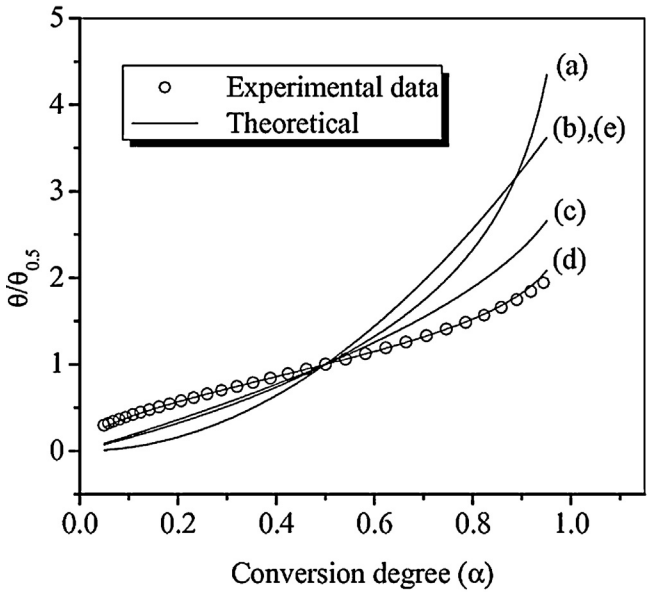

Fig. 11. Integral method for comparison of experimental data with representative models for decomposition of solids, Table 6. (a) F1, (b) P2, (c) R2, (d) A2, and (e) D1.

was obtained by the integral analysis, although differential and combined ones resulted in the same conclusions (not shown).

From Fig. 11 the best fitting of experimental data was obtained with the mechanism A2 (Avrami-Erofeyev with second order kinetic). Neither the reaction order (F1), diffusion (D1), geometrical contraction (R2), and power (P2) law models nor another models such A3, A4, P2 nor F2 (see Ref. [44]) were in agreement to the experimental data. Models P2 and D1 had almost the same profile. Eq. (17) that represents the model A2 is based on the nucleation principle, which is propitiated by solid imperfections, since activation energy is lower in these points, known as nucleation sites. Reaction (R2) corresponds to the model A2, where the solid "*A*" decomposes by thermal effects into solid "*B*" and a gas "*C*"; the nucleation process comes from the formation of a new phase of product *B*, on the nucleation sites, in the vicinity of reactant *A* [44]. Although the power law and autocatalytic Praut–Tompkins models also belong to nucleation mechanism, the Avrami-Erofeyev takes into account some restrictions for the nucleus growing such as ingestion and coalescence. The ingestion eliminates a potential nucleation site by the growing of an already occurring nucleus. In the coalescence process, there is a loss of reactant or product in the interface when reaction zones of two or more growing nucleus are converging [44]. These results also confirm formic acid is hardly observed under nitrogen conditions [32], and that autocatalytic mechanism promoted by formic acid was not operative under tested conditions, coherently with the proposed chain-end mechanism when HCHO is obtained as the main compound.

$$\frac{d\alpha}{dt} = 2 \times k \times (1-\alpha)\{-\ln(1-\alpha)\}^{1/2} \quad (17)$$

$$A_{(s)} \rightarrow B_{(s)} + C_{(g)} \quad (R2)$$

3.2.4. Kinetic model determination for PFS

As the decomposition mechanism for PFS is complex (Section 3.2.2), the Master Plot method was used in a short reaction conversion interval, $\Delta\alpha$, taking eleven points, $\Delta\alpha/11$. In this way, it is possible to obtain kinetic schemes for multiple reactions. Thus, the activation energy was taken as constant for $\Delta\alpha = 0.01$ in the

range of α between 0.03 and 0.98, and the aforementioned methods (Section 3.2.3) were used in the same intervals where E_α is considered constant. The Master Plot method associates each value of the activation energy to the best model, and it does not take into account a pattern or distinguish the components into apparent activation energy. Then the integral form of the generalized kinetic, Eq. (18), was used.

$$\frac{g(\alpha)}{g(\Delta\alpha/2)} = \frac{\theta}{\theta_{\Delta\alpha/2}} \tag{18}$$

with $(\alpha_i - \Delta\alpha) < \alpha \leq \alpha_i$ in a step of $\Delta\alpha/n$, $\Delta\alpha = 1/m$, and $i = 1, 2, 3, \ldots, n$; where n and m are arbitrary values that depend on each programmer.

Similarly to the calculations with PFP, the integral method was used for a better estimation. Since, graphical comparisons are tedious, a non-linear correlation, Eq. (19), was used to determine the best model.

$$r = \sqrt{1 - \frac{\mathrm{SSR}}{\mathrm{SST}}} \tag{19}$$

where SSR is the residual sum of squares and SST is the total sum of squares.

Fig. 12 shows the best correlated models obtained at different heating rates for each α, where three regions are observed. In the first region, the relatively high correlation (0.99 for $\beta = 7.5\,^{\circ}\mathrm{C\,min^{-1}}$), exhibited a fast reduction to values of around $r = 0.90$; in this zone, the geometrical contraction is dominant, and as PF is spherical the model R3 was selected. In the second region, r increased slowly up to about 1, when conversion values depended on heating rate. Finally, in the third region, r was close to 1, and almost constant. The last two zones are dominated by the model A2, which is the same of PFP.

According to Fig. 12, it is possible to suggest that at the beginning of PFS depolymerization a fast nucleation process occurs on its surface and that the depolymerization rate is controlled by the progress of resulting surface reaction toward the center of the solid [44]. After this process, the model A2 becomes more significant every time but with an important contribution of model R3, until the third zone ($\alpha = 0.45$, 0.55 and 0.70, for $\beta = 5$, 7.5 and $10\,^{\circ}\mathrm{C\,min^{-1}}$, respectively). This trend was attributed to the fact that at lower heating rates, there is enough time for the geometrical contraction occurs at the beginning of the reaction, and the achievement of higher temperatures, where A2 model is operative, takes longer times. In other words, the geometrical contracting is favored at low temperatures, although its activation energy is bigger, because the geometry of the solid plays an important role in the kinetics.

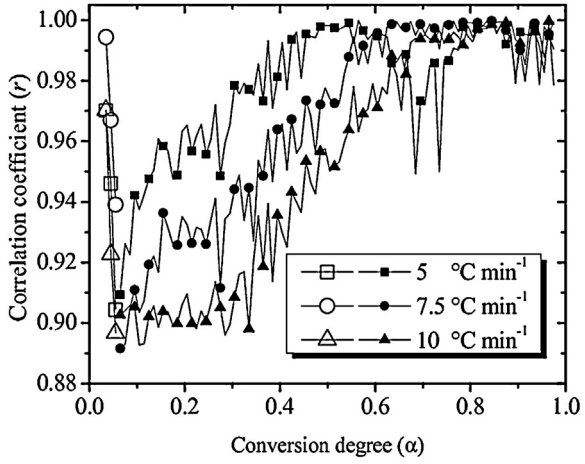

Fig. 12. Best correlation coefficients of fitted models to PFS as function of conversion and heating rate. Model R3 (open symbols), and model A2 (filled symbols).

Considering the parallel processes described by R3 and A2 models that describe the start and the end of the analysis, respectively, the activation energies obtained were 101 and $50\,\mathrm{kJ\,mol^{-1}}$, respectively.

3.2.5. Validation of kinetics for PFP

Kinetic parameters obtained in Section 3.2.1 were compared with the variance (S^2), Eq. (20) [38].

$$S^2 = \frac{\mathrm{SSR}}{N - p} \tag{20}$$

where N is the number of experimental points and p is the number of kinetic parameters for fitting. The most suitable parameters should have the lowest S^2 [39].

Table 7 shows the variance and kinetic parameters for integral and differential models which were evaluated in Section 3.2.1. These calculations came from comparison of each experimental data in TG with predicted ones using the corresponding models. Parameters obtained by Kissinger method were clearly the best from statistical point of view. Coherently, Fig. 13 shows a good prediction of experimental data using Avrami-Erofeyev-2 (A2) model with Arrhenius parameters from Kissinger method. Then, other fitting parameters procedures were not necessary. (Table 7) (Fig. 13)

From Fig. 13 is concluded that thermal depolymerization of PFP is governed by the nucleation Avrami-Erofeyev A2 model, with $E_a = 31.7\,\mathrm{kJ\,mol^{-1}}$ and $A = 1682\,\mathrm{min^{-1}}$ that were determined by the Kissinger method.

3.2.6. Validation of kinetics for PFS

Parameters for R3 and A2 models, which were preliminarily proposed from Fig. 13 in decomposition of PFS, did not agree with experimental data according to variance parameter (Table 8). Optimization of the objective function, Eq. (21), was carried out in the whole conversion range with E_a initial values of 101 and $50\,\mathrm{kJ\,mol^{-1}}$, for R3 and A2 models, respectively. After optimization, the variances were of the same order of magnitude when PFP was evaluated (Tables 7 and 8). The optimized E_a were 105.4 and $48.4\,\mathrm{kJ\,mol^{-1}}$ for R3 and A2 models, respectively. In spite of initial values were a gross estimate of the Arrhenius parameters, they were close to the boundaries of the optimized values. These results confirmed the sensibility of the prediction respect to Arrhenius parameters. So, complex decomposition processes requires special attention on Arrhenius parameters to obtain acceptable prediction by the models.

$$\mathrm{OF} = \sum_{j=1}^{m} (r_{je} - r_{jc})^2 \tag{21}$$

where m is the number of experimental points of different heating rates, e corresponds to experimental value, and c to values obtained with Eq. (10).

Table 7
Variances and kinetic parameters of different isoconversional models in depolymerization of PFP.

Method	Heating rate, β, (°C min^{-1})			Kinetic parameters	
	5.0	7.5	10.0	E, kJ mol^{-1}	A, min^{-1}
Kissinger	9.00×10^{-5}	1.44×10^{-4}	8.22×10^{-5}	31.7	1682
Integral KAS	4.85×10^{-3}	6.17×10^{-3}	5.53×10^{-3}	30.8	1760
Differential FR	2.02×10^{-2}	2.28×10^{-2}	5.53×10^{-3}	31.5	3252
Farjas	3.37×10^{-1}	3.72×10^{-1}	5.53×10^{-3}	32.5	54

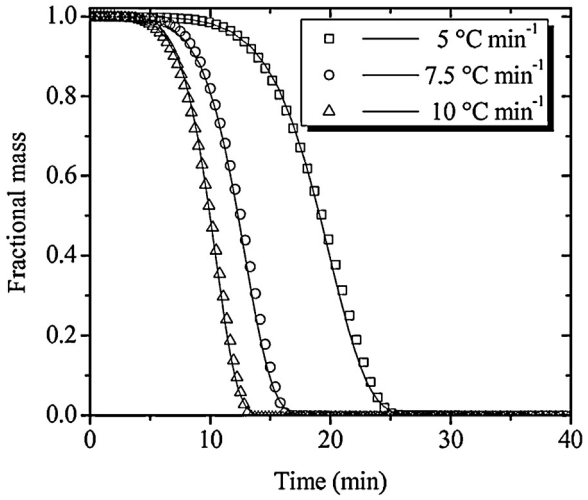

Fig. 13. Prediction of depolymerization profile of PFP using model A2 and kinetic parameters from Kissinger method. Symbols for experimental data and continuous line for simulated profiles.

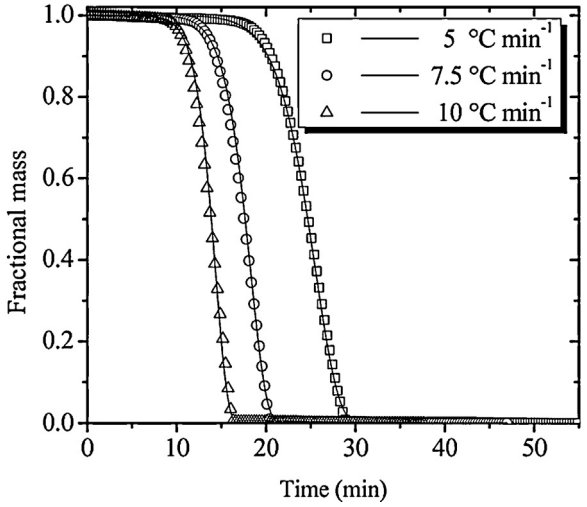

Fig. 14. Prediction of depolymerization profile of PFS using optimized kinetic parameters for the parallel reactions models R3 and A2. Symbols for experimental data and continuous line for simulated profiles.

In accordance with Table 8, Fig. 14 shows a good agreement among experimental and simulated data using the optimized Arrhenius parameters, and considering R3 and A2 mechanism occurring simultaneously. It is logical to consider that because of the spherical form of the polymer, it reacted first over its surface and next toward its core; besides, while that last process occurred, the produced smaller nucleus began to react with a mechanism A2, like the case of PFP.

Fig. 15 shows the ratio among the normalized reaction rates of R3 and A2. It is outstanding the vertical axis for R3 was thousand times higher than for A2 in the beginning of the decomposition. The ratio between the reaction rates of R3 and A2 was in the following descending order: 10 °C min^{-1} (5.8×10^{11}) > 7.5 °C min^{-1} (1800) > 5.0 °C min^{-1} (500). These calculations were in agreement with Fig. 12 where model R3 is dominating in the first steps, but at relatively short time the model A2 governed the decomposition process.

If we consider the model A2, the activation energy for PFP (31.7 kJ mol^{-1}) is lower than that obtained for PFS (48.4 kJ mol^{-1}); moreover, the decomposition of two different POM-H sources resulted in even higher activation energies (81 and 99 kJ mol^{-1}), whose differences were attributed to the length of the chain of polymers or the impurities in the sample [14]. As it was discussed earlier (Section 3.1.2), differences in our samples are attributed to a higher polymerization degree of PFS. Lüft et al. [42] reviewed the typical published activation energy values for POM; the authors found that there is a relatively broad range of reported values (16–290 kJ mol^{-1}), and that they depend on whether the POM is stabilized or nor, the molecular weight distribution, the dominating depolymerization mechanism, and the measurement methods. Moreover, the activation energy would depend on whether the decomposition atmosphere is oxygen or nitrogen, being coherently lower in the presence of oxygen [42]. To carry out a better comparison, we compared the values reported for POM-H; with exception of the works of Fray et al. (81–99 kJ mol^{-1}) [14], and Dudina et al. (108.8 kJ mol^{-1}) [62], which experiments were done in absence of oxygen, the studies have been usually carried out under thermooxidative conditions. Grassie and Roche [11] found that activation energy for the thermooxidative degradation of a high molecular weight POM-H increases from 20 to 30 kJ mol^{-1} in the early stages to 210–220 kJ mol^{-1} from about 40% volatilization onwards. Quite similar to our experiments, Kern and Cherdron [16] found an activation energy of 41.8 kJ mol^{-1} for a PF sample (molecular weight ≈ 1000 Da), which increased to 126 ± 18 kJ mol^{-1} (calculated with the reported data and assuming pseudo-first order decomposition) for a POM-H (molecular weight ≈ 10,000 Da), indicating the effect of polymer weight on the end-chain scission mechanism. The latter value is higher than the corresponding polymer but with an end-capping treatment in which dimethyl ether terminal was introduced, and whose values were 60.7 kJ mol^{-1} and 117 kJ mol^{-1} for thermooxidative and thermal degradation under vacuum, respectively [16]. Differences of values reported for the aforementioned PF samples respect to present study could be ascribed either to the observed pattern between carrying out decomposition in oxygen or nitrogen, or to differences on molecular weights.

Table 8
Effect of kinetic parameters of R3 and A2 models on variance for prediction of decomposition profiles of PFS.

β, (°C min^{-1})	S^2 with parameters in Section 3.2.2	S^2 after optimization
5.0	0.04119	4.7402×10^{-5}
7.5	0.03996	9.2051×10^{-5}
10.0	0.04168	1.3390×10^{-4}

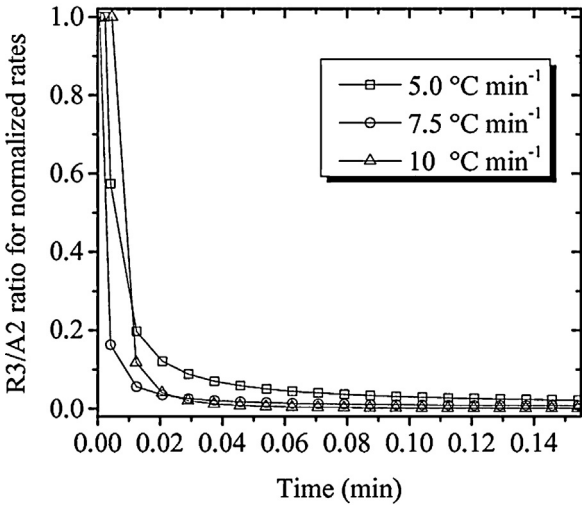

Fig. 15. Normalized rate ratio between models R3 and A2.

Additionally, it is important to note that depolymerization rate and models on PFP and PFS obtained by TGA are qualitatively in agreement to differences on nopol production shown in Table 1. HCHO is more readily available from PFP, and important differences on activity were not observed by changing particle sizes. In contrast, PFS decreased the rate of formation of HCHO, and the most important is the reduction on nopol production after increasing PFS particle size, this in agreement to geometrical volume contraction model R3, whose depolymerization rate is inversely related to particle radius [44], because the reduction of particle size causes an increase of solid reactivity. For nopol production, the main effect of the solvent has been attributed to HCHO solubility and to solvation of bulk species and intermediates [63]. Although, it is also necessary to evaluate the probable effect of the acidity of catalyst surface on the acidolytic cleavage of PF, its low solubility in organic solvents does not favored neither diffusion nor its subsequent adsorption on the acid sites, and the PF kinetics of thermal depolymerization could be also used for kinetic studies of nopol production.

4. Conclusions

The depolymerization kinetics of two sources of HCHO polymers has different behavior under TGA experiments at constant heating rate. Paraformaldehyde powder decomposition occurs in a single step by Avrami-Erofeyev (A2) model with activation energy of 31.7 kJ mol^{-1}, and paraformaldehyde prills show two simultaneous decomposition models: geometrical contraction (R3) and Avramy-Erofeyev (A2) with activation energies of 105.4 and 48.4 kJ mol^{-1}, respectively. Analysis of parallel degradation mechanism of paraformaldehyde prills was based on a modification of the Master Plot method, in which small conversion intervals were selected for evaluation. A lower HCHO production rate is predicted for paraformaldehyde prills by TGA, which is also in agreement with catalytic activity in a typical anhydrous liquid phase reaction, where *in situ* HCHO is condensed with β-pinene to obtain nopol. The geometrical contraction model, included in the complex depolymerization mechanism of paraformaldehyde prills, is in agreement with the low nopol formation as the particle size is increased. Summarizing, this study showed the versatility of TGA to evaluate the effect of the characteristics of the polymer on its depolymerization kinetic that can influence the reactivity of the obtained monomer in the further reaction steps where it is used as reactant.

Acknowledgements

This work was supported by "Departamento Administrativo de Ciencias, Tecnología e Innovación COLCIENCIAS" Contract RC-0572-2012-Bio-Red-Co-CENIVAM and Universidad de Antioquia (UdeA) Sustainability Strategy 2013–2014. E.J.G. is grateful to COLCIENCIAS and UdeA the internship grant funding through the "Programa de Jóvenes Investigadores e Innovadores (617, 2013)".

References

[1] J. Kim, B.D. Kay, Z. Dohna'lek, Formaldehyde polymerization on $(WO_3)_3$ /TiO_2 (110) model catalyst, J. Phys. Chem. C 114 (2010) 17017–17022, doi:http://dx.doi.org/10.1021/jp102710m.
[2] Merchant Research & Consulting Ltd. World Formaldehyde Production to Exceed 52 Mln Tonnes in 2017, June 27. (2014). http://mcgroup.co.uk/news/20140627/formaldehyde-production-exceed-52-mln-tonnes.html (accessed 1.15.15).
[3] G. Reuss, W. Disteldorf, A.O. Gamer, A. Hilt, Formaldehyde, Ullmann's Encyclopedia of Industrial Chemistry, Wiley-VCH, Weinheim, 2000, pp. 1–34, doi:http://dx.doi.org/10.1002/14356007 a11_619 (online ed).
[4] I.M. Pastor, M. Yus, The Prins reaction: advances and applications, Curr. Org. Chem. 11 (2007) 925–957, doi:http://dx.doi.org/10.2174/138527207781024067.
[5] E.A. Alarcón, A.L. Villa, Sóntesis de nopol a partir de trementina: revisión del estado del arte, Ing. Cienc. 8 (2012) 281–305. http://search.ebscohost.com/login.aspx?direct=trhttp://publicaciones.eafit.edu.co/index.php/ingciencia/article/view/1715.
[6] E. Alarcón, A.L. Villa, C. Montes de C, Producción de nopol con Sn-MCM-41 sintetizada hidrotérmicamente, Proc. XXI Simp. Iberoam. Catálisis, Málaga, España, 2008.
[7] E. Alarcón, A.L. Villa, C. Montes de Correa, Efecto de las condiciones de síntesis hidrotérmica de Sn-MCM-41 en la producción de nopol, Rev. Fac. Ing. Univ. Antioquia. 49 (2009) 19–29.
[8] D.A. Skoog, F.J. Holler, T.A. Nieman, Principios de Analisis Instrumental, 5a ed., McGraw-Hill Interamericana de España S.L., 2001.
[9] C.E. Schweitzer, R.N. MacDonald, J.O. Punderson, Thermally stable high molecular weight polyoxymethylenes, J. Appl. Polym. Sci. 1 (1959) 158–163.
[10] S. Igarashi, I. Mita, H. Kambe, Thermogravimetric analysis of polyoxymethylene, Bull. Chem. Soc. Jpn. 37 (1964) 1160–1165, doi:http://dx.doi.org/10.1246/bcsj.37.1160.
[11] N. Grassie, R.S. Roche, The thermal degradation of polyoxymethylene, Die Makromol. Chem. 112 (1968) 16–33, doi:http://dx.doi.org/10.1021/ja01228a061.
[12] M. Hasegawa, K. Yamamoto, T. Shiwaku, T. Hashimoto, Formation of macrocyclic poly(oxymethylene) with narrow molecular weight distribution on the lamellar crystals, Macromolecules 23 (1990) 2629–2636, doi:http://dx.doi.org/10.1021/ma00212a006.
[13] V.M. Archodoulaki, S. Lüftl, S. Seidler, Thermal degradation behaviour of poly (oxymethylene): 1. Degradation and stabilizer consumption, Polym. Degrad. Stab. 86 (2004) 75–83, doi:http://dx.doi.org/10.1016/j.polymdegradstab.2004.03.011.
[14] N. Fray, Y. Bénilan, H. Cottin, M.C. Gazeau, New experimental results on the degradation of polyoxymethylene: application to the origin of the formaldehyde extended source in comets, J. Geophys. Res. 109 (2004) , doi:http://dx.doi.org/10.1029/2003JE00219.
[15] R.P. Kusy, J.Q. Whitley, Degradation of plastic polyoxymethylene brackets and the subsequent release of toxic formaldehyde, Am. J. Orthod. Dentofacial Orthop. 127 (2005) 420–427, doi:http://dx.doi.org/10.1016/j.ajodo.2004.01.023.
[16] V.W. Kern, H. Cherdron, Der Abbau von Polyoxymethylenen, Die Makromol. Chem. 40 (1960) 101–117.
[17] O. Vogl, V. Ivansons, H.C. Miller, H.W. Williams, Thermal degradation spectrum; instrumentation to record thermogravimetric results, J. Macromol. Sci. Part A – Chem. 2 (1968) 175–181, doi:http://dx.doi.org/10.1080/00222336808053355.
[18] Polyoxymethylene Handbook – Structure, Properties, Applications and Their Nanocomposites, in: S. Lüft, P.M. Visakh, S. Chandran (Eds.), Scrivener Publishing LLC, Massachusetts, 2014.
[19] F.J. Gotor, J.M. Criado, J. Malek, N. Koga, Kinetic analysis of solid-state reactions: the universality of master plots for analyzing isothermal and nonisothermal experiments, J. Phys. Chem. A 104 (2000) 10777–10782, doi:http://dx.doi.org/10.1021/jp0022205.
[20] T. Kitazawa, H. Tadokoro, T. Matsumoto, I. Imazu, The relation between infrared spectra and degree of polymerization of polyoxymethylene and molecular orientation in film samples, Kobunshi Kagaku 19 (1962) 148–153, doi:http://dx.doi.org/10.1295/koron1944.19.148.
[21] H. Tadokoro, M. Kobayashi, Y. Kawaguchi, A. Kobayashi, S. Murahashi, Normal vibrations of the polymer molecules of helical configuration. III. Polyoxymethylene and polyoxymethylene-d_2, J. Chem. Phys. 38 (1963) 703–721, doi:http://dx.doi.org/10.1063/1.1733727.
[22] C. Lorthioir, F. Lauprêtre, K. Sharavanan, R.F.M. Lange, P. Desbois, M. Moreau, et al., Solid-state organization and morphological partitioning in polyoxymethylene-based copolymers: a solid-state NMR and WAXS study, Macromolecules 40 (2007) 5001–5013, doi:http://dx.doi.org/10.1021/ma062507l.
[23] H. Luo, Y. Huang, D. Wang, Confined crystallization of POM in the CA-nanotubes fabricated by coaxial electrospinning, Eur. Polym. J. 49 (2013) 1424–1436, doi:http://dx.doi.org/10.1016/j.eurpolymj.2013.02.037.
[24] T. Kitagawa, T. Miyazawa, Neutron scattering and normal vibrations of polymers, Adv. Polym. Sci. 9 (1972) 335–414, doi:http://dx.doi.org/10.1007/3-540-05484-7.
[25] M. Kobayashi, H. Morishita, M. Shimomura, M. Iguchi, Vibrational spectroscopic study on the solid-state phase transition of poly (oxymethylene) single crystals from the orthorhombic to the trigonal phase, Macromolecules 20 (1987) 2453–2456, doi:http://dx.doi.org/10.1021/ma00176a021.
[26] H. Hama, K. Tashiro, Structural changes in non-isothermal crystallization process of melt-cooled polyoxymethylene. [I] Detection of infrared bands characteristic of folded and extended chain crystal morphologies and extraction of a lamellar stacking model, Polymer (Guildf) 44 (2003) 3107–3116, doi:http://dx.doi.org/10.1016/S0032-3861(03) 207-6.
[27] M. Shimomura, M. Iguchi, M. Kobayashi, Vibrational spectroscopic study on trigonal polyoxymethylene and polyoxymethylene-d_2 crystals, Polymer (Guildf) 29 (1988) 351–357, doi:http://dx.doi.org/10.1016/0032-3861(90)90141-K.

[28] M. Shimomura, M. Iguchi, Infra-red study on the conformational regularity in needle-like and other polyoxymethylene crystals, Polymer (Guildf) 23 (1982) 509–513, doi:http://dx.doi.org/10.1016/0032-3861(82) 90090-8.
[29] Principles and Applications of Thermal Analysis, in: P. Gabbott (Ed.), Blackwell Publishing, 2007.
[30] K. Pielichowski, A. Leszczynska, TG-FTIR study of the thermal degradation of polyoxymethylene (POM)/thermoplastic polyurethane (TPU) blends, J. Therm. Anal. Calorim. 78 (2004) 631–637, doi:http://dx.doi.org/10.1023/B:JTAN 46124.19405. aa.
[31] V.V. Rajan, R. Wäber, J. Wieser, Online monitoring of the thermal degradation of POM during melt extrusion, J. Appl. Polym. Sci. 115 (2010) 2394–2401, doi: http://dx.doi.org/10.1002/app.
[32] Y. Duan, H. Li, L. Ye, X. Liu, Study on the thermal degradation of polyoxymethylene by thermogravimetry-fourier transform infrared spectroscopy (TG-FTIR), J. Appl. Polym. Sci. 99 (2006) 3085–3092, doi: http://dx.doi.org/10.1002/app.22913.
[33] C. Wang, X. Zhang, Y. Liu, D. Che, Pyrolysis and combustion characteristics of coals in oxyfuel combustion, Appl. Energy 97 (2012) 264–273, doi:http://dx. doi.org/10.1016/j.apenergy.2012.02.011.
[34] M. Mucha, Thermooxidation rate of diacetate terminated polyoxymethylene with various morphological structures, Colloid Polym. Sci. 262 (1984) 841–850, doi:http://dx.doi.org/10.1007/BF01452213.
[35] Properties and Behavior of Polymers, in: A. Seidel (Ed.), first ed., John Wiley & Sons Ltd., Hoboken, NJ, 2011.
[36] T. Kongkhlang, K.R. Reddy, T. Kitano, T. Nishu, K. Tashiro, Cocrystallization phenomenon of polyoxymethylene blend samples between the deuterated and hydrogenated species, Polym. J. 43 (2011) 66–73, doi:http://dx.doi.org/ 10.1038/pj.2010.106.
[37] B. Fayolle, J. Verdu, M. Bastard, D. Piccoz, Thermooxidative ageing of polyoxymethylene, Part 1: chemical aspects, J. Appl. Polym. Sci. 107 (2008) 1783–1792, doi:http://dx.doi.org/10.1002/app.
[38] B. Janković, M. Marinović-Cincović, V. Jovanović, S. Samaržija-Jovanović, G. Marković, The comparative kinetic analysis of non-isothermal degradation process of acrylonitrile-butadiene and ethylene-propylene-diene rubber compounds. Part I, Thermochim. Acta 543 (2012) 295–303, doi:http://dx. doi.org/10.1016/j.tca.2011.11.034.
[39] S. Vyazovkin, A.K. Burnham, J.M. Criado, L.A. Pérez-Maqueda, C. Popescu, N. Sbirrazzuoli, ICTAC Kinetics Committee recommendations for performing kinetic computations on thermal analysis data, Thermochim. Acta 520 (2011) 1–19, doi:http://dx.doi.org/10.1016/j.tca.2011.03.034.
[40] S. Vyazovkin, Evaluation of activation energy of thermally stimulated solid-state reactions under arbitrary variation of temperature, J. Comput. Chem. 18 (1997) 393–402, doi:http://dx.doi.org/10.1002/(SICI)1096-987X(199702) 18:3<393::AID-JCC9>3.0.CO;2-P.
[41] J. Farjas, N. Butchosa, P. Roura, A simple kinetic method for the determination of the reaction model from non-isothermal experiments, J. Therm. Anal. Calorim. 102 (2010) 615–625, doi:http://dx.doi.org/10.1007/s10973-010-0737-5.
[42] S. Lüftl, V.M. Archodoulaki, S. Seidler, Thermal-oxidative induced degradation behaviour of polyoxymethylene (POM) copolymer detected by TGA/MS, Polym. Degrad. Stab. 91 (2006) 464–471, doi:http://dx.doi.org/10.1016/j. polymdegradstab.2005.01.029.
[43] J.H. Flynn, L.A. Wall, A quick, direct method for the determination of activation energy from thermogravimetric data, Polym. Lett. 4 (1966) 323–328, doi: http://dx.doi.org/10.1002/pol.1966.110040504.
[44] A. Khawam, D.R. Flanagan, Solid-state kinetic models: basics and mathematical fundamentals, J. Phys. Chem. B 110 (2006) 17315–17328, doi: http://dx.doi.org/10.1021/jp062746a.
[45] S. Vyazovkin, N. Sbirrazzuoli, Isoconversional kinetic analysis of thermally stimulated processes in polymers, Macromol. Rapid Commun. 27 (2006) 1515–1532, doi:http://dx.doi.org/10.1002/marc.200600404.
[46] S. Vyazovkin, D. Dollimore, Linear and nonlinear procedures in isoconversional computations of the activation energy of nonisothermal reactions in solids, J. Chem. Inf. Model. 36 (1996) 42–45, doi:http://dx.doi.org/10.1021/ci950062m.
[47] S. Vyazovkin, Modification of the integral isoconversional method to account for variation in the activation energy, J. Comput. Chem. 22 (2001) 178–183, doi: http://dx.doi.org/10.1002/1096-987X(20010130)22:2<178::AID-JCC5>3.0. CO;2-#.
[48] N. Sbirrazzuoli, Is the Friedman method applicable to transformations with temperature dependent reaction heat? Macromol. Chem. Phys. 208 (2007) 1592–1597, doi:http://dx.doi.org/10.1002/macp.200700100.
[49] P. Budrugeac, Differential non-linear isoconversional procedure for evaluating the activation energy of non-isothermal reactions, J. Therm. Anal. Calorim. 68 (2002) 131–139, doi:http://dx.doi.org/10.1023/A:1014932903582.
[50] S. Vyazovkin, A unified approach to kinetic processing of nonisothermal data, Int. J. Chem. Kinet. 28 (1996) 95–101, doi:http://dx.doi.org/10.1002/(SICI) 1097-4601(1996) 28:2<95::AID-KIN4>3.0. CO;2-G.
[51] E. Bonnet, R.L. White, Species-specific isoconversion effective activation energies derived by thermogravimetry–mass spectrometry, Thermochim. Acta 311 (1998) 81–86, doi:http://dx.doi.org/10.1016/S0040-6031(97)00411-5.
[52] S.V. Vyazovkin, A.I. Lesnikovich, An approach to the solution of the inverse kinetic problem in the case of complex processes. Part 1. Methods employing a series of thermoanalytical curves, Thermochim. Acta 165 (1990) 273–280, doi: http://dx.doi.org/10.1016/0040-6031(90)80227-P.
[53] S.V. Vyazovkin, V.I. Goryachko, A.I. Lesnikovich, An approach to the solution of the inverse kinetic problem in the case of complex processes. Part III. Parallel independent reactions, Thermochim. Acta 197 (1992) 41–51, doi:http://dx.doi. org/10.1016/0040-6031(92)87037-B.
[54] S. Vyazovkin, Conversion dependence of activation energy for model DSC curves of consecutive reactions, Thermochim. Acta 236 (1994) 1–13, doi: http://dx.doi.org/10.1016/0040-6031(94)80249-1.
[55] S. Vyazovkin, W. Linert, Kinetic analysis of reversible thermal decomposition of solids, Int. J. Chem. Kinet. 27 (1995) 73–84, doi:http://dx.doi.org/10.1002/ kin.550270109.
[56] S. Vyazovkin, An approach to the solution of the inverse kinetic problem in the case of complex processes: Part 4. Chemical reaction complicated by diffusion, Thermochim. Acta 223 (1993) 201–206, doi:http://dx.doi.org/10.1016/0040-6031(93)80135-W.
[57] F.S. Dainton, K.J. Ivin, D.A.G. Walmsley, The equilbrium between gaseous formaldehyde and solid polyoxymethylene, Trans. Faraday Soc. 55 (1959) 61–64, doi:http://dx.doi.org/10.1039/tf9595500061.
[58] J.F. Walker, Formaldehyde, third ed., Reinhold Publishing Corporation, New York, 1964.
[59] O. Vogl, Kinetics of aldehyde polymerization, J. Macromol. Sci. Part C: Polym. Rev. 12 (1975) 109–164, doi:http://dx.doi.org/10.1080/15321797508076105.
[60] J. Málek, The kinetic analysis of non-isothermal data, Thermochim. Acta 200 (1992) 257–269, doi:http://dx.doi.org/10.1016/0040-6031(92)85118-F.
[61] J.H. Flynn, The temperature integral – its use and abuse, Thermochim. Acta 300 (1997) 83–92, doi:http://dx.doi.org/10.1016/S0040-6031(97)00046-4.
[62] L.A. Dudina, L.V. Karmilova, E.K. Tryapitsyna, N.S. Enikolopyan, The kinetics and mechanism of thermal and thermal-oxidative degradation of formaldehyde polymers, J. Polym. Sci. Part C 16 (1967) 2277–2288.
[63] D. Casas-Orozco, E. Alarcón, A.L. Villa, Kinetic study of the nopol synthesis by the Prins reaction over tin impregnated MCM-41 catalyst with ethyl acetate as solvent, Fuel 149 (2015) 130–137, doi:http://dx.doi.org/10.1016/j. fuel.2014.08.067.